Environmental and Experimental Biology (2025) 23: 95–102
http://doi.org/10.22364/eeb.23.10

Original Paper

Synergizing field measurements and handheld LiDAR for estimating carbon stocks in mixed deciduous forest on a river island in lower northern Thailand

ISSN 2255-9582

Tinnapan Netae[1], Pativit Sarapin[1], Nataporn Meesawat[2], Rutairat Phothi[1]*

[1]Environmental Science Program, Faculty of Science and Technology, Nakhon Sawan Rajabhat University, Thailand
[2]Physic and General Science Program, Faculty of Science and Technology, Nakhon Sawan Rajabhat University, Thailand

*Corresponding author, E-mail: rutairat.p@nsru.ac.th

Abstract

This study explores the application of handheld 3D LiDAR technology to assess aboveground biomass and carbon storage of large trees within a mixed deciduous forest ecosystem. The research was conducted on a river island in the lower northern region of Thailand. The total area of the river island is approximately 4.16 ha. A total of 235 large trees from 17 species were inventoried within ten plots located in a mixed deciduous forest on a river island. Tree structural characteristics, such as diameter at breast height and total height were measured using conventional field techniques alongside handheld LiDAR scanning to enable cross-method comparisons. Allometric equations were applied to estimate total biomass and carbon stock. The results revealed strong correlations between LiDAR-derived and field-based measurements of diameter at breast height, height, and CO_2 sequestration, with R^2 values exceeding 0.98. The combined aboveground and belowground biomass totaled 126.933 tons, and the estimated average CO_2 adsorption was 547.37 t ha^{-1}. *Bombax ceiba* exhibited the highest CO_2 sequestration among all trees. Additionally, soil carbon stock averaged 5.06 t ha^{-1}, with the greatest concentration observed at a depth of 50 cm. These findings demonstrate that handheld LiDAR is a reliable and efficient tool for forest carbon assessment in isolated ecosystems.

Key words: carbon stock, handheld 3D LiDAR, mixed deciduous forest, river island.
Abbreviations: AGB, aboveground biomass; BGB, belowground biomass; DBH, diameter at breast height; LiDAR, light detection and ranging.

Introduction

Climate change is a phenomenon driven by global warming, primarily caused by the use of fossil fuels such as coal, oil, and natural gas in human activities. Since the industrial revolution in 1800, the combustion of fossil fuels has consistently released greenhouse gases into the atmosphere, including carbon dioxide (CO_2), methane, nitrous oxide, hydrofluorocarbons, perfluorocarbons, sulfur hexafluoride, and nitrogen trifluoride. Among these, CO_2 is particularly significant as a greenhouse gas. The global average atmospheric concentration of CO_2 was 280 ppm prior to the industrial revolution and around 419.30 ppm in 2023 (Climate.gov 2024). CO_2 concentrations in the atmosphere simulated by models range between 470 – 570 ppm and 730 –1020 ppm in 2050 and 2100, respectively (IPCC 2007). By the late 21st century, the global temperature predicted under the IPCC scenario will increase by another 2.6 to 4.8 °C (IPCC 2013). The global temperature increase is likely causing alterations in parts of the water cycle. It is leading to more frequent and severe weather phenomena such as heatwaves, storms, droughts, and floods. Considering the intensifying climate crisis, the Paris Agreement articulates a scientifically grounded objective to constrain the rise in global mean temperature to below 1.5 °C by 2100. This target is nested within a broader international commitment to achieve net-zero greenhouse gas emissions, stabilizing Earth's climate system through long-term decarbonization trajectories (Chen et al. 2025).

Light detection and ranging (LiDAR) technology offer a fast and high-precision method for capturing and creating 3D models of the real world. It detects objects by emitting rapid laser pulses and using sensors to measure the time it takes for those pulses to bounce back after hitting surfaces (Raj et al. 2020). LiDAR point clouds can be used to accurately estimate treetops, diameter at breast

height, canopy size, other structural attributes, which can be used to calculate the trees number per unit area. These LiDAR-derived structural attributes can be combined with field measurements to estimate forest aboveground biomass and forest aboveground carbon stock using various models. Handheld LiDAR scanning is a mobile 3D laser scanning technology that has become a practical and efficient tool for forest inventory and tree mapping. Recent research has demonstrated that handheld LiDAR scanning delivers comparable accuracy to terrestrial laser scanning when detecting tree positions and estimating key structural attributes. Most studies have focused on assessing the accuracy and operational efficiency of both handheld LiDAR scanning and terrestrial laser scanning technologies in measuring fundamental tree metrics, particularly diameter at breast height (DBH) and tree height (Lin et al. 2012; Ryding et al. 2015; Stal et al. 2021; Yang et al. 2024). Handheld LiDAR scanning offers better portability and faster data collection than terrestrial laser scanning and is easier to operate in dense or remote forests, which makes it suitable for rapid ecological assessments. Although handheld LiDAR scanning has shown promising accuracy in measuring individual tree attributes like DBH and height, its effectiveness depends on factors such as canopy density and understory clutter (Bauwens et al. 2016; Proudman et al. 2022). For example, Maan et al. (2015) also highlighted that terrain complexity greatly influences LiDAR-derived forest metrics, especially in hilly tropical areas. Moreover, recent studies have emphasized the need for site-specific calibration and consideration of ecological context when applying handheld LiDAR across different forest types (Tupinamba-Simoes et al. 2025). These findings highlight the need for localized validation studies, particularly in underrepresented ecosystems such as Southeast Asian forests. Furthermore, isolated river island forests have unique ecological and structural features that remain insufficiently studied. Although handheld LiDAR is increasingly used in forest inventories, its integration with field-based data for assessing carbon stocks across components such as tree biomass and soil carbon remains limited.

This research aimed to evaluate the correlation between field-based measurements and handheld LiDAR scanning derived estimates of DBH and height of trees for carbon sequestration evaluation in large trees on a river island. It also investigated tree species diversity and the potential for soil carbon storage across study plots within mixed deciduous forests on river island ecosystems in the lower northern region of Thailand.

Materials and methods

Study area

The study area was located on an island in the Ping River (15°56'19"N, 99°59'00"E) within Banphot Phisai District, Nakhon Sawan Province, Thailand covering an area of approximately 26 rai or 41 600 m^2. Since 2010, this site had been designated as a local conservation area under the Plant Genetic Conservation Project initiated by Her Royal Highness Princess Maha Chakri Sirindhorn. The area exhibited a forest cover of approximately 95%, with elevations around 47.97 m above sea level. Due to the disconnection of access routes, the island had been isolated from human activity for over a decade and during the study. In 2022, the average daily temperatures range from 23.67 to 33.95 °C with a mean annual temperature average of 28.31 °C (Nakhon Sawan Provincial Statistical Office 2023).

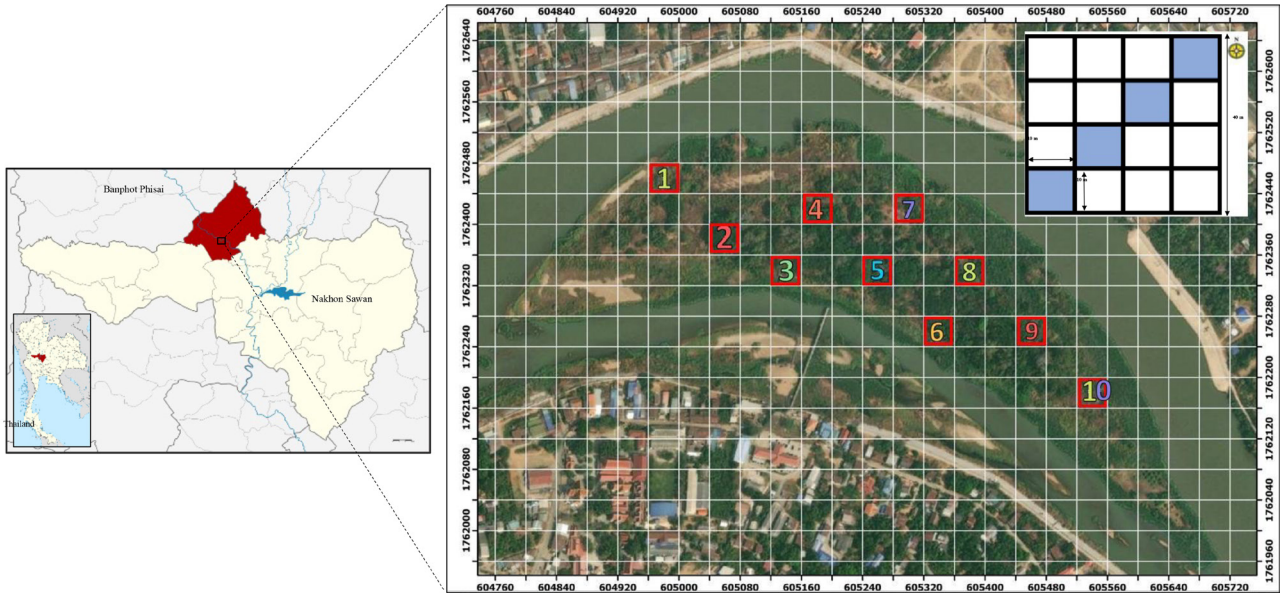

Fig. 1. Sample plot layout for inventory of large trees on an island in the Ping River within Banphot Phisai District, Nakhon Sawan Province, Thailand.

Tree data

The field work was undertaken in April 2024. A total of ten 40 × 40 m plots were systematically distributed throughout the study site to enable a comprehensive assessment of vegetation composition and structural characteristics. Within each main plot, tree data were recorded from four nested subplots of 10 × 10 m (Fig. 1).

The identification of large tree species at least 1.3 m in height with DBH 4.5 cm was carried out with assistance from a tree taxonomist and the scientific names were confirmed using the World Flora Online database (WFO 2021). The species diversity, evenness and richness of forest were assessed in accordance with Ludwig and Reynolds (1988), including Shannon-Weiner diversity index (H'), Pielou's evenness index (J), and Margalef richness index (R_1) based on the formulas presented in equations 1, 2, and 3, respectively:

$$H' = -\sum pi\ (\ln p_i)\ (1),$$
$$J = H / \ln S\ (2),$$
$$R_1 = (S - 1) / \ln (n)\ (3),$$

where p_i is the proportion of a specific tree species (i) recorded within a plot, n indicates the total number of individuals found in the plot, and S is the number of species.

The total biomass (TB) was estimated using allometric equations tailored to the specific vegetation structure and species found in the mixed deciduous or dipterocarp forests (Ogawa et al. 1961). All trees in the observation plots were identified at the species level. Trees were counted. Height (H) and diameter (D) at 1.30 m was used for estimating aboveground biomass (AGB) and belowground biomass (BGB). Each tree height measurement was derived from a laser rangefinder (Nikon Forestry Pro II) and only trees exceeding 1.30 m in height and having a diameter at breast height of at least 4.5 cm were considered in the analysis. The AGB was derived by summing the estimated masses of stems, branches, and foliage. BGB or root biomass was estimated using root/shoot ratio of 0.26. The allometric equations 4 to 9 were used to determine the total biomass TB as follows:

$$W_S = 0.0396\ (D^2H)^{0.9326}\ (4),$$
$$W_B = 0.00349\ (D^2H)^{1.030}\ (5),$$
$$W_L = [28 / (WS + WB + 0.025)]^{-1}\ (6),$$
$$AGB = WS + WB + WL\ (7),$$
$$BGB = 0.26\ AGB\ (8),$$
$$T_B = AGB + BGB\ (9),$$

where W_S, W_B, and W_L represent the biomass in kg of the stem, branches, and leaves, respectively.

The carbon content of biomass was calculated and converted into CO_2 adsorption. Carbon content (CCt) and CO_2 absorption assessments were carried out following the methodology developed by Haghdoost et al. (2013) and Girma et al. (2014), respectively. The calculations were as follows:

$$CCt = 0.5\ T_B\ (10),$$
$$CO_2\ absorption = 3.67\ CCt\ (11).$$

The total carbon adsorption within the conservation area was calculated from the sum of CO_2 adsorption of large trees in all plots.

Soil data

Soil samples were collected from all plots at depths of 15, 30, and 50 cm with a coring tool. Soil samples were air-dried at room temperature (30 °C) for three days, then manually crushed and passed through a 2-mm sieve. Estimates of total organic carbon (OC) in soil were made by the rapid titrimetric oxidation technique (Walkley, Black 1934). The principal of this technique was oxidizing organic carbon with a hot mixture of potassium dichromate ($K_2Cr_2O_7$) and concentrated sulfuric acid (H_2SO_4). The residual dichromate was determined by titration with using phenanthroline as an indicator. Bulk density was estimated using the core method following Grossman and Reinsch (2002). The bulk density of a soil is defined as the ratio of the mass of oven-dried soil core at 105 °C for 24 h to the total volume of the core, which encompasses both the soil particles and the pore spaces between them. The carbon content or CC (kg C m^{-2}) from soil depths of 15, 30, and 50 cm was calculated as in equation 12:

$$CCs = D \times V \times BD \times OC\ (12),$$

where D is soil depth (cm); V is soil volume, while BD is bulk density (g cm^{-3}) and OC is organic carbon concentration in bulk soil (%).

Total carbon content or TCCs (kg C m^{-2}) was calculated by the sum of soil carbon in each depth as described in equation 13:

$$TCCs = CCs_{15} + CCs_{30} + CCs_{50}\ (13),$$

where CCs_{15}, CCs_{30}, and CCs_{50} are the soil carbon content at 15, 30, and 50 cm depth, respectively.

Handheld LiDAR data acquisition and processing

The ICS LiPix handheld LiDAR was employed for three-dimensional data collection in the study area. This device utilizes solid-state SLAM (Simultaneous Localization and Mapping) technology to generate high-density point cloud data for vegetation structure analysis. The system utilized a solid-state LiDAR sensor from the Livox brand, which provided a non-repetitive scanning field of view measuring 70.4 degrees horizontally and 77.2 degrees vertically. Operating in single-backward mode, the sensor recorded up to 240 000-point clouds per second. This device was used to determine tree locations, measure diameter at breast height (DBH), and estimate tree height within the island study area. Data collection was conducted within the same locations as the field measurement plots or ten plots total.

Statistical analysis

Soil experiments were triplicated, and mean values were analyzed by analysis of variance (one-way ANOVA) with the post hoc Duncan test ($p < 0.05$). A comparative analysis

Table 1. Occurrence of tree species in ten sampling plots on a river island

Family	Species	Number of individuals	Frequency (%)
Moraceae	*Streblus asper* Lour.	97	41.28
Fabaceae-Caesalpinioideae	*Delonix regia* (Boj. ex Hook.) Raf.	40	17.02
Euphorbiaceae	*Bridelia ovata* Decne	24	10.21
Moraceae	*Ficus carica* L.	17	7.23
Meliaceae	*Azadirachta indica* A.Juss	13	5.53
Fabaceae-Mimosoideae	*Samanea saman* (Jacq.) Merr.	9	3.83
Fabaceae	*Leucaena leucocephala* (Lam.) de Wit	8	3.40
Moraceae	*Ficus racemosa* L.	7	2.98
Calophyllaceae	*Calophyllum inophyllum* L.	4	1.70
Fabaceae	*Pithecellobium dulce* (Roxb.) Benth	4	1.70
Rubiaceae	*Nauclea orientalis* (L.) L.	3	1.28
Malvaceae	*Bombax ceiba* L.	3	1.28
Fabaceae	*Albizia lebbeckoides* (DC.) Benth.	2	0.85
Fabaceae	*Senna siamea* (Lam.) Irwin et Barneby	1	0.43
Lythraceae	*Lagerstroemia floribunda* Jack	1	0.43
Fabaceae	*Peltophorum pterocarpum* (DC.) K.Heyne	1	0.43
Euphorbiaceae	*Trewia nudiflora* L.	1	0.43
	Total	235	100

between field-based measurements and LiDAR derived estimates was conducted using regression modeling to evaluate the accuracy of tree height, DBH, and CO_2 sequestration estimates. The coefficient of determination (R^2) was used to assess model performance.

Results and discussion

Tree diversity indices

The survey area contained 235 large trees representing 17 species from 10 families. The frequency classes showed that *Streblus asper* and *Delonix regia* were the most dominant species, and together they represented 58.30 % of the total population observed in the survey area (Table 1).

The analysis revealed that the diversity, evenness, and richness of large trees on the Ping River island in Banphot Phisai District reached 2.00, 0.71, and 2.93, respectively. In the context of Asian forest ecosystems, the diversity, evenness, and richness observed here were lower than in natural forests but exceeded those found in community-managed areas (Table 2).

Table 2. Tree diversity data in island in comparison with other forests in Asian countries

Country, region	Forest	Area	Diversity (H')	Evenness (J)	Richness (R_1)	Reference
Western Indonesia	Tropical rain forest	Barumun watershed forest in north Sumatra province	2.24	0.70	23.83	Rambey et al. 2021
		Titi Kembar Rivulet watershed forest in north Sumatra province	1.42	0.88	4.54	
Eastern Nepal	Tropical forest	Non-disturbed forest in Koshi province	3.08	0.76	9.11	Gautam, Mandal 2018
		Disturbed forest in Koshi province	2.80	0.77	6.78	
Northern Thailand	Mixed deciduous forest	Four community forests in Uttaradit province	1.13	0.55	1.87	Podong, Krivutthinun 2018
			0.59	0.29	1.80	
			0.83	0.40	1.59	
			1.09	0.52	2.73	
Northern Thailand	Mixed deciduous forest	Waterfall forest park in Chiang Rai province	3.58	0.671	7.27	Nukool 2002
Lower northern Thailand	Mixed deciduous forest	Island on the river in Nakhon Sawan provice	2.00	0.71	2.93	The present study

Table 3. Biomass, carbon content, and CO2 adsorption of 17 different tree species from ten sampling plots on an island. AGB, aboveground biomass; BGB, belowground biomass; ACC, aboveground carbon content; BCC, belowground carbon content; CCt, carbon content

Species	AGB (kg)	BGB (kg)	Biomass (kg)	ACC (kg)	BCC (kg)	CCt (kg)	Adsorption (kg CO_2)
Streblus asper	10 413.04	2707.39	13 120.43	4894.13	1272.47	6166.60	22 631.43
Delonix regia	16 311.83	4241.08	20 552.91	7666.56	1993.31	9659.87	35 451.71
Bridelia ovata	647.98	168.47	816.45	304.55	79.18	383.73	1408.30
Ficus carica	6743.51	1753.31	8496.82	3169.45	824.06	3993.51	14 656.17
Azadirachta indica	1827.28	475.09	2302.37	858.82	223.29	1082.12	3971.36
Samanea saman	35 985.94	9356.34	45 342.28	16 913.39	4397.48	21 310.87	78 210.91
Leucaena leucocephala	336.48	87.48	423.96	158.15	41.12	199.26	731.30
Ficus racemosa	2997.11	779.25	3776.36	1408.64	366.25	1774.89	6513.84
Calophyllum inophyllum	105.07	27.32	132.39	49.38	12.84	62.22	228.36
Pithecellobium dulce	933.22	242.64	1175.86	438.61	114.04	552.65	2028.24
Nauclea orientalis	842.93	219.16	1062.09	396.18	103.01	499.18	1832.00
Bombax ceiba	20 306.42	5279.67	25 586.09	9544.02	2481.44	12 025.46	44 133.45
Albizia lebbeckoides	352.37	91.62	443.99	165.61	43.06	208.67	765.83
Senna siamea	1120.72	291.39	1412.11	526.74	136.95	663.69	2435.74
Lagerstroemia floribunda	93.20	24.23	117.42	43.80	11.39	55.19	202.54
Peltophorum pterocarpum	49.60	12.89	62.48	23.31	6.06	29.37	107.78
Trewia nudiflora	1673.86	435.20	2109.06	786.71	204.55	991.26	3637.92
Total	100 740.56	26 192.53	126 933.07	47 348.05	12 310.50	59 658.54	218 946.88

Biomass and CO_2 adsorption efficiency

The mean biomass and CO_2 adsorption efficiency of the different tree species is shown in Table 3. Results show that the combined aboveground and belowground biomass of large trees across the sampling plots was 126 933 kg. The three species exhibiting the greatest total biomass were *Samanea saman, Bombax ceiba*, and *Delonix regia*. These species accounted for approximately 72% of the total biomass recorded, underscoring their ecological significance in carbon storage within the study area. Bombax ceiba exhibited the highest CO_2 adsorption among recorded species in the study area or 14 711 kg tree^{-1}, followed by *Samanea saman* (8690 kg tree^{-1}) and *Trewia nudiflora* (3638 kg tree^{-1}), respectively. The carbon content according to the mature trees on the island was 6115 t or approximately 149.15 t carbon ha^{-1}. The overall average CO_2 adsorption across all tree compartments was 22 442 t CO_2 or approximately 547 t CO_2 ha^{-1} (Fig. 2).

The total biomass values observed in this study align closely with those reported for mature trees in a previous study by Raha et al. (2020), indicating consistency with established findings in similar forest contexts. The results of this study indicate that the mixed deciduous forest examined is likely a primary mixed deciduous forest because of a carbon stock that is higher than 50 t carbon ha^{-1} (Chaiyo et al. 2012). It was demonstrated that aboveground biomass carbon in primary mixed deciduous forests of the lower northern region of Thailand was significantly greater than that of secondary forests, with values approximately 2.5 times higher (Kaewkrom et al. 2011).

As individual trees develop over time, they gradually absorb carbon dioxide from the air and convert it through photosynthesis. The resulting carbon compounds are stored in plant tissues and contribute to biomass (Nunes et al. 2020). The value of CO_2 adsorption efficiency estimated for the mature trees on the island is higher than those previously documented in mixed deciduous forests of Thailand, which range from 48 to 103 t CO_2 ha^{-1} (Pinmongkhonkul et al. 2023; Chandaeng et al. 2020; Chaiyo et al. 2011). These findings reinforce the important role of mature trees in long-term carbon sequestration and suggest a consistent pattern of carbon storage capacity across similar forest types.

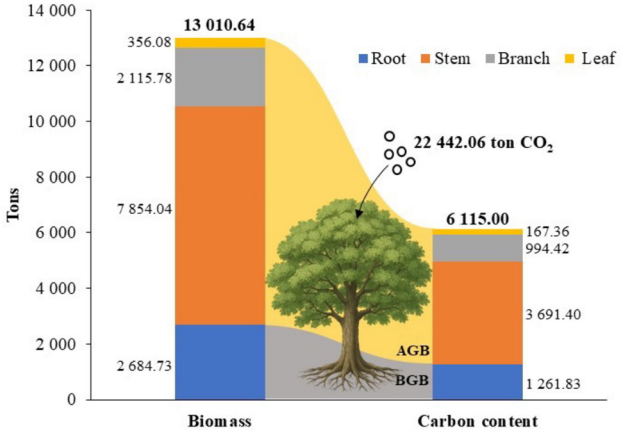

Fig. 2. Total carbon content from stem, branch leaf, and root biomass of large trees from island.

Table 4. Mean carbon stock influenced by variations in volume (V), bulk density (BD), and organic carbon (OCs) at 15, 30, and 45 cm soil depths (D) from ten sampling plots on an island. Mean followed by different letters are significantly different ($p < 0.05$)

D (cm)	V (m^3)	BD (mg cm^{-3})	OCs (%)	Carbon stock in soil (t C ha^{-1})
15	240	2.18 ± 0.14 a	1.39 ± 0.14 c	0.72 ± 0.12 a
30	480	5.37 ± 0.11 c	0.72 ± 0.08 b	1.86 ± 0.25 b
50	800	4.87 ± 0.12 b	0.63 ± 0.03 a	4.87 ± 0.12 c

Carbon stock in soil

The results revealed that OC in soil from the island decreased with increasing depth, while the bulk density measurements indicated that the highest values occurred at the 30 cm depth interval at 5.37 mg cm^{-3} and showed a slight decline at 50 cm depth. Following the calculations, it was evident that carbon stock distribution varied with soil depth. The highest carbon accumulation was observed at 50 cm depth, and progressively lower amounts were detected at 30 cm and 15 cm depths, respectively. The total carbon stock in soil on an island was 5.06 t C ha^{-1} or approximately 207 416 kg (Table 4).

A significant portion of OC in forest soils lies below 20 cm, with up to 50% stored down to 1 m and an additional 56% potentially found between 100 and 300 cm depth (Jobbágy, Jackson 2000). This vertical distribution pattern aligns with several studies conducted in forested ecosystems, which reported that deeper soil layers can contribute substantially to total soil organic carbon stocks. For instance, Li et al. (2022) found that in a subtropical agricultural watershed, only 19% of total OC was stored in the top 30 cm of soil, while over 63% was found below 100 cm. Similarly, Byers et al. (2023) reported that in a radiata pine plantation, more than 35% of OC was accumulated below 30 cm depth, and carbon in these deeper layers exhibited greater stability and older age. These findings underscore the importance of subsoil in long-term carbon sequestration, especially in undisturbed or semi-natural ecosystems such as the river island examined in the present study.

Correlation between field-based measurements and handheld LiDAR scanner derived estimates

The scan performed by the handheld LiDAR scanner detected 236 trees. This number was very close to the 235 trees recorded in the ground truth data and showed the highest consistency in tree detection among all point cloud datasets. Tree height and DBH derived from 3D point clouds using merged portable on-ground LiDAR data within the sampling plots are shown in Fig. 3. The resulting values were subjected to correlation analysis with tree height and DBH obtained from field measurements.

Fig. 4 illustrates the correlation analysis between tree attributes derived from handheld LiDAR scanner and those measured on the ground, revealing a high correlation between them. Fig. 4A presents the correlation between tree height measured in the field using a laser rangefinder and height estimated automatically from the handheld LiDAR scanner. The relationship between tree height measured in the field using a laser rangefinder and height estimated from LiDAR data followed a curvilinear pattern described by the equation $y = 2.2605\ e^{0.0937}$. The intercept value of 2.2605 reflects the average condition index of the trees, while the exponential rate $e^{0.0937}$ represents the trend in tree height growth (R^2 value of 0.98). In general, tree height values derived from handheld LiDAR were systematically underestimated when compared with field-based measurements. The analysis revealed a high linear relationship between DBH values obtained using a diameter tape and those measured by the handheld LiDAR scanner. The coefficient of determination was R^2 value

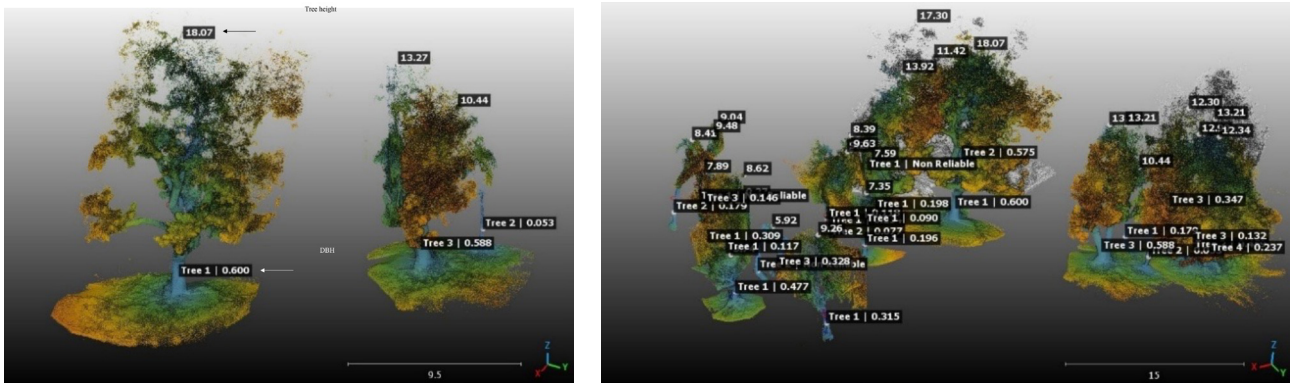

Fig. 3. The tree height and diameter at breast height (DBH) in the 3D point cloud images of trees in the sampling plots by merging portable on-ground scanning LIDAR data.

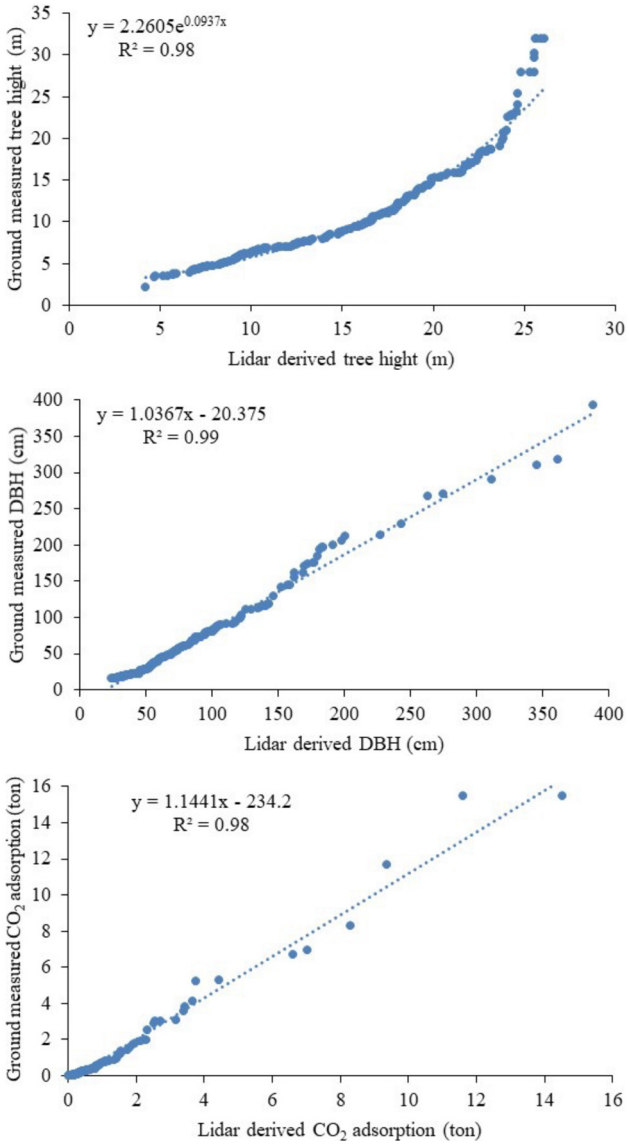

Fig. 4. Correlation between field measurements and handheld LiDAR data for tree height (A), diameter at breast height (B), and CO_2 sequestration in large trees (C).

of 0.99 as shown in Fig. 4B. The correlation between the field CO_2 sequestration and LIDAR predicted in the large trees was good, with an r^2 value of 0.98 (Fig. 4C). The linear relationship between LiDAR-derived and ground-measured CO_2 adsorption was represented by the equation

$$y = 1.1441x - 234.2,$$

where y denotes the CO_2 adsorption measured in the field (kg) and x represents the value estimated from LiDAR data (kg).

Handheld LiDAR scanning demonstrates strong potential for accurately capturing forest structural attributes and minimizing uncertainty in aboveground biomass estimation, as it enables detailed measurement of complete tree volume. This approach has been shown to detect more than 90% of trees and provides highly consistent DBH estimates when compared to ground-based methods (Mak et al. 2025). Although handheld LiDAR involves higher initial costs than traditional field methods. It significantly reduces the time required for data collection, making it a more efficient choice for large-scale forest assessments (Tantrairatn et al. 2025).

Conclusions

This study explores the potential of handheld LiDAR scanning as a practical and precise tool for assessing forest carbon and structural analysis in ecologically complex environments. The integration of handheld LiDAR data with field measurements improves the accuracy and operational efficiency of biomass and carbon stock estimation. The findings demonstrate the ecological importance of river island forests and their contribution to carbon sequestration. Such approaches offer valuable support for sustainable forest monitoring and contribute to the broader understanding of ecosystem dynamics in Southeast Asia.

Acknowledgements

The authors gratefully acknowledge the financial support provided by Nakhon Sawan Rajabhat University, Thailand. This support was instrumental in facilitating the successful completion of the research.

References

Bauwens S., Bartholomeus H., Calders K., Lejeune P. 2016. Forest inventory with terrestrial LiDAR: A comparison of static and hand-held mobile laser scanning. *Forests* 7: 127.

Chaiyo U., Garivait S., Wanthongchai K. 2012. Structure and carbon storage in aboveground biomass of mixed deciduous forest in western region, Thailand. *GMSARN Int. J.* 6: 143–150.

Chen W.-H., Biswas P.P., Zhang C., Kwon E.E., Chang J.-S. 2025. Achieving carbon credits through biomass torrefaction and hydrothermal carbonization: A review. *Renew. Sustain. Energy Rev.* 208: 115056.

Climate.gov. 2024. Climate change: Atmospheric carbon dioxide. National Oceanic Atmosphere Administration. https://www.climate.gov/news-features/understanding-climate/climate-change-atmospheric-carbon-dioxide

Gautam T.P., Mandal T.N. 2018. Effect of disturbance on plant species diversity in moist tropical forest of eastern Nepal. *Our Nature* 16: 1–7.

Girma A., Soromessa T., Bekele T. 2014. Forest carbon stocks in woody plants of Mount Zequalla Monastery and its variation along altitudinal gradient: Implication of managing forests for climate change mitigation. *Sci. Technol. Arts Res. J.* 3: 132–140.

Grossman R.B., Reinsch T.G. 2002. Bulk density and linear extensibility. In: Dane J.H., Topp G.C. (Eds.) *Methods of Soil Analysis: Part 4. Physical Methods.* Soil Science Society of America, pp. 201–228.

Haghdoost N., Akbarinia M., Hosseini S.M. 2013. Land–use change and carbon stocks: A case study, Noor County, Iran. *J.*

Forest Res. 24: 461–469.

IPCC. 2007. *Climate Change 2007: The Physical Science Basis*. Contribution of Working Group I to the Fourth Assessment Report of the Intergovernmental Panel on Climate Change. Cambridge University Press.

IPCC. 2013. *Climate change 2013: The Physical Science Basis*. Contribution of Working Group I to the Fifth Assessment Report of the Intergovernmental Panel on Climate Change. Cambridge University Press.

Kaewkrom P., Kaewkla N., Thummikkapong S., Punsang S. 2011. Evaluation of carbon storage in soil and plant biomass of primary and secondary mixed deciduous forests in the lower northern part of Thailand. *African J. Environ. Sci. Technol.* 5: 8–14.

Lin Y., Hyyppä J., Kukko A., Jaakkola A., Kaartinen H. 2012. Tree height growth measurement with single-scan airborne, static terrestrial and mobile laser scanning. *Sensors* 12: 12798–12813.

Ludwig J.A., Reynolds J.F. 1988. *Statistical Ecology: A Primer on Methods and Computing.* Wiley.

Maan A.A., Ibrahim A.N.H., Ahmed O.H. 2015. Impact of topography and LiDAR-derived metrics on aboveground biomass estimation in tropical forests. *Geocarto Int.* 30: 293–310.

Nakhon Sawan Provincial Statistical Office. 2023. Nakhon Sawan Provincial Statistical Report 2023. National Statistical Office.

Nukool T. 2002. Structural characteristics of three forest types at KhunKorn Waterfall Forest Park, Changwat Chiang Rai. Master's thesis. Kasetsart University.

Nunes L.J.R., Meireles C.I.R., Pinto Gomes C.J., Almeida Ribeiro N.M.C. 2020. Forest contribution to climate change mitigation: Management oriented to carbon capture and storage. *Climate* 8: 21.

Ogawa H., Yoda K., Ogino K., Kira T. 1961. Comparative ecological studies on three main types of forest vegetation in Thailand: I. Structure and floristic composition. *Nat. Life Southeast Asia* 1: 129–204.

Pinmongkhonkul S., Boonriam W., Madhyamapurush W., Iamchuen N., Chaiwongsaen P., Mann D., Riyamongkol P., Seetapan K., Hasin S. 2023. Species diversity, aboveground biomass, and carbon storage of watershed forest in Phayao Province, Thailand. *Environ. Nat. Resour. J.* 21: 47–57.

Podong C., Krivutthinun P. 2018. Tree species richness and diversity of community forestry in Uttaradit Province, Thailand. *Nat. Environ. Pollut. Technol.* 17: 87–92.

Proudman M., Lo C.Y., Cai Z., Lane D.M. 2022. Tree mapping using mobile LiDAR systems in natural forests: Advances and limitations. *Robotics Auton. Syst.* 157: 104240.

Raj T., Hashim F., Huddin A.B., Ibrahim M.F., Hussain A. 2020. A survey on LiDAR scanning mechanisms. *Electronics* 9: 741.

Raha D., Dar J., Pandey P., Lone P., Verma S., Khare P.K., Khan M. 2020. Variation in tree biomass and carbon stocks in three tropical dry deciduous forest types of Madhya Pradesh, India. *Carbon Manage.* 11: 1–12.

Rambey R., Susilowati A., Rangkuti A., Onrizal O., Desrita D., Ardi R., Hartanto A. 2021. Plant diversity, structure and composition of vegetation around Barumun Watershed, North Sumatra, Indonesia. *Biodiversitas* 22: 3250–3256.

Ryding J., Williams E., Smith M., Eichhorn M. 2015. Assessing handheld mobile laser scanners for forest surveys. *Remote Sens.* 7: 1095–1111.

Stal C., Verbeurgt J., De Sloover L., De Wulf A. 2021. Assessment of handheld mobile terrestrial laser scanning for estimating tree parameters. *J. Forest Res.* 32: 1503–1513.

Tantrairatn S., Pichitkul A., Petcharat N., Karaked P., Ariyarit A. 2025. Evaluating LiDAR technology for accurate measurement of tree metrics and carbon sequestration. *MethodsX* 14: 103237.

Tupinambá-Simões F., Pascual A., Guerra-Hernández J., Ordóñez C., Barreiro S., Bravo F. 2025. Combining hand-held and drone-based lidar for forest carbon monitoring: insights from a Mediterranean mixed forest in central Portugal. *Eur. J. Forest Res.* 144: 925–940.

Walkley A., Black I.A. 1934. An examination of the Degtjareff method for determining soil organic matter and a proposed modification of the chromic acid titration method. *Soil Sci.* 37: 29–38.

WFO. 2021. World Flora Online. http://www.worldfloraonline.org (Accessed April 30, 2023)

Yang J., Yuan W., Lu H., Liu Y., Wang Y., Sun L., Li S., Li H. 2024. Assessing the performance of handheld laser scanning for individual tree mapping in an urban area. *Forests* 15: 575.

Received 20 May 2025; received in revised form 27 June 2025; accepted 5 September 2025